THE JOURNAL OF PHYSICAL CHEMISTRY C

Article

Cite This: J. Phys. Chem. C 2018, 122, 10181−10188

pubs.acs.org/JPCC

Pushing the Boundaries of Interfacial Sensitivity in Graphene FET Sensors: Polyelectrolyte Multilayers Strongly Increase the Debye Screening Length

Esteban Piccinini,[*,†,⊥] Sebastián Alberti,[†,⊥] Gabriel S. Longo,[†] Teresa Berninger,[‡] Josef Breu,[§] Jakub Dostalek,[‡] Omar Azzaroni,[*,†] and Wolfgang Knoll[‡]

[†]Instituto de Investigaciones Fisicoquímicas Teóricas y Aplicadas (INIFTA)−Departamento de Química, Facultad de Ciencias Exactas, Universidad Nacional de La Plata−CONICET, Suc. 4, CC 16, La Plata, Argentina

[‡]AIT Austrian Institute of Technology, Donau City Strasse 1, 1220 Vienna, Austria

[§]Inorganic Chemistry I, University of Bayreuth, 95440 Bayreuth, Germany

Supporting Information

ABSTRACT: Nanomaterial-based FET sensors represent an attractive platform for ultrasensitive, real-time, and label-free detection of chemical and biological species. Nevertheless, because their response is screened by mobile ions, it remains a challenge to use them to sense in physiological ionic strength solutions. In this work, it is demonstrated, both experimentally and theoretically, that polyelectrolyte multilayers are capable of increasing the sensing range of graphene-based FETs. Potential shifts at graphene surfaces and film thickness are recorded upon the construction of PDADMAC/PSS polyelectrolyte multilayer (PEM) films. By correlation of the potential shift with the film thickness, the electrostatic screening length and the concentration of mobile ion inside the films have been deduced. Across the polymer interface the Debye length is increased more than 1 order of magnitude. The fundamentals of this strategy are described by a conceptually simple thermodynamic model, which accounts for the entropy loss of ion confinement and incorporates the effect of ions finite volume. Interestingly, the electrostatic screening inside the film strongly depends on the polymer density and the ionic strength of the solution. Of particular interest in physiological condition sensing, the PEM interfaces can extend the Debye length from 0.8 to 10 nm.

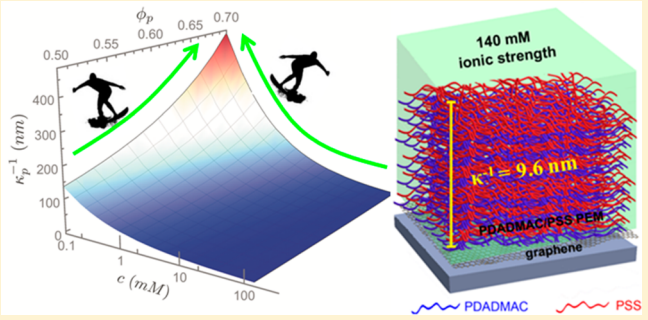

1. INTRODUCTION

Field-effect transistor (FET) biosensors based on nanomaterials such as semiconducting nanowires,[1] single-walled carbon nanotubes, and graphene[2] offer outstanding capabilities for label-free high-sensitivity real-time detection of biological species.[3] In particular, solution-gated FET biosensors have gained increasing attention in clinical diagnostics.[4] Since the first report of real-time protein detection,[1] these devices have proven high sensitivity to diverse analytes of paramount significance in biotechnology and health care: small organic molecules,[5−7] proteins,[8,9] nucleic acids,[10,11] and viruses.[12] Furthermore, they were successfully applied for the investigation of small molecule−protein interactions,[7] the enzyme-catalyzed reactions,[6] and biomolecular association/dissociation processes.[10]

Nevertheless, the use of nanomaterial-based FETs for sensing of samples in physiological solution is still behind expectations as their applications have been mainly limited to measurements in relatively low ionic strength solutions.[2,3,13] These sensors are primarily sensitive to the electrostatic potential induced by charged biomolecules, which is screened by mobile ions present in the analyzed sample.[14] On a certain length scale, termed the Debye length (κ^{-1}), surface charges are neutralized by mobile counterions. If κ^{-1} is smaller than the distance between the captured target analyte and the FET surface, then the sensor becomes insensitive to these binding events. The electrostatic screening of physiological solutions typically reduces the FET sensing range to distances below 1 nm.[3] This value is far below the size of the majority of analytes of interest such as medium and large molecular proteins with a hydrodynamic radius up to 10 nm. In addition, the distance of the analyte from the surface is also limited by the thickness of a biointerface with immobilized receptors for their specific capture which typically yields several nanometers. This inherent distance mismatch of liquid-gated FET biosensors complicates real-time detection in clinical samples.

Major research efforts have been focused on overcoming this limitation. First, a two-step method comprising an initial

Received: November 10, 2017
Revised: January 18, 2018
Published: January 22, 2018

DOI: 10.1021/acs.jpcc.7b11128
J. Phys. Chem. C 2018, 122, 10181−10188

desalting step followed by detection of disease marker proteins in low ionic strength solution was reported.[9] This method allowed for efficient detection; however, the desalting step is not suitable for real-time detection. Other groups have used small receptors to reduce the distance between the FET surface and the analyte.[15−17] Nevertheless, this method is not applicable for the detection of large biomolecules (larger than 1 nm). A high-frequency measurement strategy that can be applied to standard biological receptors was also reported.[18,19] In this case, a setup including devices of complex geometry is required, which may hinder their applicability, especially for implantable analyte level monitoring applications.

More recently, Gao et al. reported that the effective screening length in immediate proximity to the FET surface can be increased by the use of a poly(ethylene glycol) polymer layer.[8,20] This observation was demonstrated to enable detecting of prostate specific antigen (PSA) in samples with physiological ionic strength by employing silicon nanowire and graphene-based FETs. This approach holds potential to solve the problem of the mismatch between Debye length and distances dictated by the size of biomolecules. Although the authors suggested that this phenomenon might be based on the decrease of the dielectric constant of the medium by the polymer interface, the mechanisms underlying the reported behavior are still a subject of debate. In particular, some questions remain unexplained: What role do the mobile ions inside the polymer interface play in terms of electrostatic screening? How much could the Debye length be extended? Can the Debye length be tuned by the properties of the polymer interface? The present work presents experimental and theoretical results to shed further light on these issues. Changes of potential at the graphene surface as well as the film thickness were followed during the construction of polyelectrolyte multilayer (PEM) films. These measurements were performed electronically by reduced graphene oxide (rGO) FET and optically by surface plasmon resonance (SPR) combined with optical waveguide spectroscopy (OWS). Correlating these measurements, the Debye length and mobile ion concentration inside the polymer film were obtained. Notably, polyelectrolyte multilayer films offered extending the ionic screening length by more than 1 order of magnitude (see Scheme 1). PEM water content was calculated by OWS. A theoretical model is presented to explain the polymer interface behavior varying the bulk ionic strength and polymer density. The model takes into account the loss of entropy associated with the confinement of ions inside the film and is in quantitative agreement with our experimental results. Moreover, this model does not require ions to balance the polymer charge. Thus, the partition of ions inside the film results purely from entropic contributions, which allows extending our findings to explain the results of previous works.

Scheme 1. Representation of the Debye Screening Length (κ^{-1}) at a Graphene Interface for a 140 mM Ionic Strength Solution (i.e., Physiological Ionic Strength) without (Left) and with (Right) a PDADMAC/PSS Polyelectrolyte Multilayer (PEM) Film

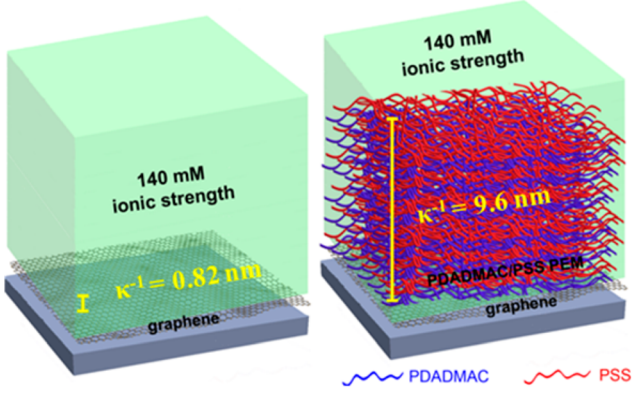

2. EXPERIMENTAL SECTION

2.1. Reduced Graphene Oxide Field-Effect Transistors. Reduced graphene oxide (rGO) field-effect transistors were prepared as previously described.[6] The rGO acted as the transistor channel, and an Ag/AgCl electrode was used as a gate. Liquid-gated graphene FET measurements were carried out using a batch-cell (from Micrux Technologies) at 1 mM or 10 mM KCl and 0.1 mM HEPES adjusted at pH 7.0. The current between the source and drain electrodes (I_{ds}) was measured as a function of the gate potential (V_g) while the potential between the drain and the source (V_{ds}) was fixed at 100 mV (see Scheme S1). Electrical measurements were performed by means of a probe station (Keithley 4200). The charge carrier mobilities (μ) of the devices were 30 $cm^2\ V^{-1}\ s^{-1}$ for holes and 15 $cm^2\ V^{-1}\ s^{-1}$ for electrons, determined as described previously.[6]

2.2. Layer-by-Layer Assembly. In order to confer negative charge to the graphene surface, the rGO FETs were modified with sodium 1-pyrenesulfonate (SPS) as previously described.[6] Layer-by-layer (LbL) assemblies mediated by electrostatic interactions were built up onto the SPS-modified rGO FETs by alternate adsorption of poly(diallyldimethylammonium chloride) (PDADMAC, M_w < 100 000, Sigma-Aldrich) and poly(sodium 4-styrenesulfonate) (PSS, M_w = 70 000, Sigma-Aldrich). First, the SPS-modified rGO FETs were incubated in an aqueous solution of 1 mg/mL PDADMAC for 10 min, rinsed with deionized water, and blow-dried with air. Then, the PDADMAC modified FETs were incubated in 1 mg/mL of PSS for 10 min, rinsed with deionized water, and dried with air. Polyelectrolyte multilayer assemblies were constructed by repeating the PDADMAC and PSS adsorption using two different conditions: (a) from polyelectrolyte solutions containing 0.5 M KCl and (b) from polyelectrolytes solutions without the addition of salt.

2.3. Surface Plasmon Resonance (SPR) and Optical Wave Spectroscopy (OWS). A monochromatic light beam from a He−Ne laser (PL610P, Polytec, Germany, power 2 mW, wavelength λ = 632.8 nm) was linearly polarized, passed through a chopper (Princeton Applied Research, USA) for lock-in detection, and coupled to a 90° LaSFn9 prism. Onto the prism base, a LaSFn9 glass substrate (η = 1.845) with a 2 nm layer of chromium and 50 nm layer of gold was optically matched using a high refractive index immersion oil (Cargile, USA). The intensity of the light beam that was reflected at the prism base was measured using a photodetector and a lock-in amplifier (Model 5210, Princeton Applied Research, USA). The angle of incidence, θ, of the light beam was controlled using a rotation stage (Hans Huber AG, Germany).

2.4. Graphene-Modified SPR and OWS Substrates. First, the substrates were modified with a self-assembled monolayer (SAM) of cysteamine by incubation in 5 mM cysteamine ethanolic solution for 8 h. Then, an aqueous dispersion of GO flakes was drop-cast on the substrates for 2 h.

DOI: 10.1021/acs.jpcc.7b11128
J. Phys. Chem. C 2018, 122, 10181−10188

Finally, the GO was chemically reduced by using hydrazine at 80 °C overnight. A flow-cell consisting of an O-ring and a UV−visible transparent glass bottom was attacheded to the gold surface to prepare the polyelectrolyte multilayer assemblies in situ. After each polyelectrolyte adsorption, the substrates were rinsed with deionized water, dried, and then filled with the aqueous solution for measuring. Data analysis was done with Winspall software (see the Supporting Information for more details). Refractive indexes in dry and swollen state were related to polymer/water volume content by using effective medium theory and in particular Lorenz−Lorenz relation (see the Supporting Information for more details).

3. RESULTS AND DISCUSSION

Polyelectrolyte multilayers were prepared from PDADMAC and PSS by the layer-by-layer (LbL) adsorption technique (Scheme 1). This technique offers a versatile and simple bottom-up approach for the construction of interfacial architectures with nanometer-level control over the structure, composition, and properties.[21−24] Particularly, the LbL assembly through electrostatic interactions has been firmly established as a general method for alternately depositing dense layers of charged molecules onto oppositely charged surfaces.[25] The concept of the approach relies on the attractive forces between oppositely charged macromolecules. Since graphene surface is naturally noncharged, it was modified with sodium 1-pyrenesulfonate to obtain a negatively charged basic layer. In this process, the pyrene groups attach to graphene through $\pi-\pi$ interactions whereas the oppositely positioned sulfonate groups form a negatively charged surface which is stable in a wide range of pH.[6] This composition allowed for the initiation of the LbL assembly process, in which the polyelectrolytes PDADMAC (negatively charged) and PSS (positively charged) were absorbed alternately.

3.1. Film Thickness of PEM Assembled on Graphene Surfaces. The successive growth of PEM on graphene was in situ followed optically by the combined OWS and SPR. In this method, graphene was attached to a gold surface, and the stack of polyelectrolyte layers on its top was optically probed by resonantly excited surface plasmon and optical waveguide waves. The resonant coupling to these surface waves can be observed as series of dips in transverse magnetic (TM) and transverse electric (TE) reflectivity. Figure 1a shows TM reflectivity as a function of the incidence angle (θ) after the deposition of $(PDADMAC/PSS)_n$ bilayers, with n = 0, 3, 5, and 8. The adsorption of polyelectrolytes is associated with pronounced shift in the resonant angle at which the excitation of surface plasmon (TM_0) mode occurs. This shift is proportional to the surface mass density of immobilized polymer, and by fitting of these changes by Fresnel reflectivity model, refractive index and thickness of PEM were determined. To maximize the load of the polyelectrolyte layers, we have taken advantage of the possibility of controlling the film growth in LbL assemblies by varying the ionic strength of the polyelectrolyte solutions.[26,27] Thus, multilayer films were prepared by using polyelectrolyte solutions containing high (0.5 M KCl) and low (no KCl) ionic strength. As can be seen in Figure 1a, resonance shifts ascribed to the adsorption of polyelectrolyte were higher at high ionic strength (right) than at low ionic strength (left). These shifts correspond to about 30-times higher thickness of the PEM assembly, yielding about 160 nm for the growth of n = 9 bilayers at high ionic strength

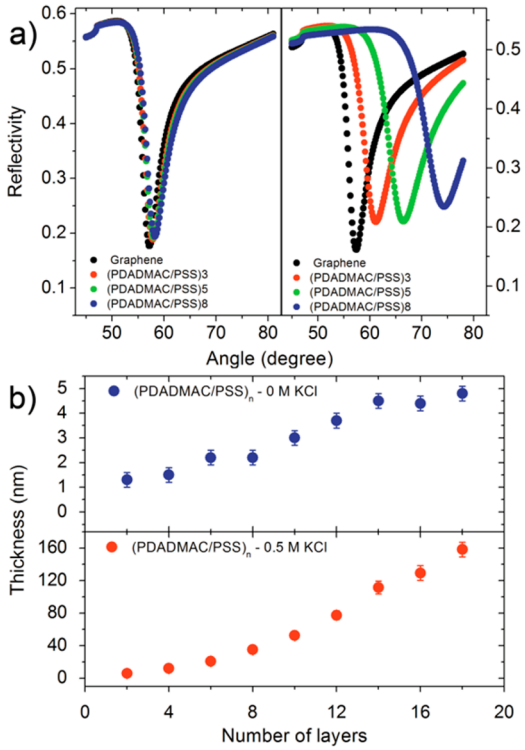

Figure 1. (a) TM reflectivity as a function of the incidence angle for $(PDADMAC/PSS)_n$ assemblies (0, 3, 5, and 8 bilayers) prepared from polyelectrolyte solutions without (left) and with (right) the addition of 0.5 M KCl. (b) Thickness as a function of the number of layers without (top) and with (bottom) the addition of 0.5 M KCl.

(right) compared to the 5 nm film thickness obtained at low ionic strength (left), see Figure 1b.

While in thin films (<150 nm) TM_0 was the only mode accessible for the probing of PEM, thicker films (>150 nm) allow the excitation of additional modes with different profile of field (TE_0 and TM_1). In the latter, both thickness and refractive index (η) can be determined independently. Figure S3a shows TM and TE for the hydrated $(PDADMAC/PSS)_{13}$ film. Refractive index value of 1.476 ± 0.005 was obtained for such thick films, and it was used for thinner films fitting that only displayed TM_0. The quantified film thickness of PEMs constructed under high and low ionic strength is summarized in Figure 1b. It reveals that the growth of PEMs constructed under high ionic strength followed a supralinear behavior (Figure 1b, bottom). Although in this work PEMs were assembled on graphene surfaces, the obtained thickness and the trend to supralinear growth are in excellent agreement with characteristics reported for PDADMAC/PSS PEMs on thiolated gold surfaces.[28] Also the strong dependence of film thickness on ionic strength was consistent with previous results for PDADMAC/PSS PEMs prepared on oxidized silicon substrates.[27] Finally, a comparison of η_{dry} and $\eta_{hydrated}$ allowed the estimation of the water uptake upon immersion of the dry PEMs in solution. The refractive index of dry $(PDADMAC/PSS)_{12}$ film was determined as 1.577 ± 0.005 (Figure S3b). After the film was hydrated, η decreased by 0.11 units based on which the water volume fraction (ϕ_w) was estimated to be 0.32 (see the Supporting Information for more details). The value of the polymer volume fraction, $\phi_p = 1 - \phi_w$, will be used later for the thermodynamic model calculations.

DOI: 10.1021/acs.jpcc.7b11128
J. Phys. Chem. C 2018, 122, 10181−10188

3.2. Tuning the Debye Screening Length of Graphene Interfaces. Following the characterization of PEM thickness, the effect of polyelectrolyte layers on the field-effect properties was studied. Figure 2a shows the transfer characteristics of a graphene-based FET after the adsorption of the first and second PDADMAC/PSS bilayer. The PEM was assembled at low (left) and high (right) ionic strength, while the field-effect measurements were performed in a 1 mM KCl solution. The assembly of a positively charged PDADMAC layer resulted in a shift of the Dirac point (V_i) to a more negative gate voltage. In contrast, the subsequent negatively charged PSS layer displaced V_i to a more positive gate voltage. An explanation has recently been given by Wang and Burke, who ascribe this field effect behavior to the induction of negative (positive) charges on graphene induced by the adsorption of positively (negatively) charged macromolecules, which ultimately leads to a shift of the Fermi energy to the conduction (valence) band.[29]

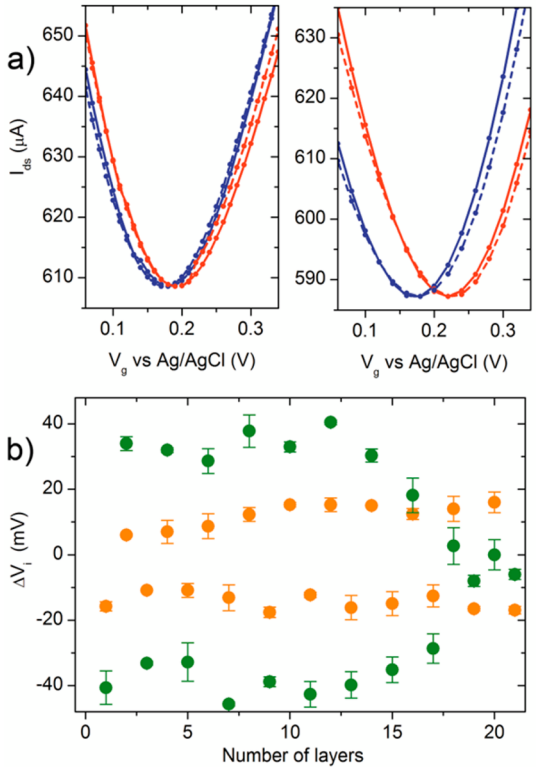

Figure 2. (a) Transfer characteristics of graphene-based FETs for PDADMAC/PSS assemblies prepared from polyelectrolyte solutions without (left) and with (rigth) the addition of 0.5 M KCl. The first and the second bilayers are represented using solid and dashed lines, respectively. PDADMAC-terminated assemblies are represented as blue lines and PSS-terminated assemblies as red lines. (b) Change of the Dirac point (ΔV_i) as a function of the number of adsorbed layers. The LbL assemblies were prepared from polyelectrolyte solution at low (orange) and high (green) ionic strength. All the field-effect experiments were performed in 1 mM KCl at V_{ds} = 0.1 V.

Dirac point shifts of −13 and −46 mV were recorded when the polycation PDADMAC was adsorbed at low and high ionic strength, respectively. After PSS deposition on the PDADMAC-modified graphene surface, the Dirac point shifted to +13 and +46 mV. For the first 10 layers, the shift of V_i was completely reversible after each layer. This is due to the charge overcompensation behavior of polyelectrolyte layer-by-layer assemblies.[30] It is important to highlight that higher V_i shifts were obtained for polyelectrolytes assembled at high ionic strength. Qualitatively, this result is easy to understand. The polyelectrolyte adsorption at high ionic strength resulted in thicker layers and, therefore, higher surface charge density (σ). Since the induced charges on graphene depend on σ,[29] a larger charge density increment is expected to yield larger ΔV_i.

The field-effect properties were measured while increasing the amount of PDADMAC/PSS layers to a maximum of 20 layers. In Figure 2b, the Dirac point changes throughout the multilayer assembly are summarized. In case of PEMs prepared at low ionic strength (orange circles), V_i reversed after each successive layer, which is in agreement with other works.[29,31] In contrast, the assemblies prepared at 0.5 M KCl (green circles) showed a damping of the absolute V_i shifts after the 12th layer. From this point on, ΔV_i decreased continuously until the 20th layer, after which there was no significant change of the Dirac point.

These results may be interpreted based on inherent physicochemical features of multilayer films as well as the FET sensing mechanism. In multilayer assemblies, polyanion/polycation complexes are formed between adjacent layers with strong interdigitation and charge overcompensation.[32] This charge overcompensation leads to a variation of the surface potential (ψ_s) at the polyelectrolyte/solution interface. On the other hand, the formation of polyanion/polycation complexes leads to low ion concentration inside the PEMs.[33−35] This implies that the Debye length inside a PEM (κ_p^{-1}) is different from the Debye length in the solution (κ_s^{-1}) (see Scheme 2b).[33,35] If PEMs are constructed onto field-effect devices, the charge overcompensation (not compensated by mobile ions) is translated into a shift of the Dirac point. Changes in the surface potential (and accordingly V_i) are strongly dependent not only on the charge density of the outermost layer but also on electrostatic screening by mobile charges within the multilayers films.[36,37] Consequently, graphene-based FETs can determine the potential drop within the films, a property that cannot be determined by zeta potential measurements.

Scheme 2. Representation of (a) the PDADMAC/PSS Polyelectrolyte Multilayer (PEM) Film, with Charge Overcompensation at the Outermost Layer, and (b) the Potential, $\psi(x)$, as a Function of the Distance, x, for a 1 mM KCl Solution and the PEM Film[a]

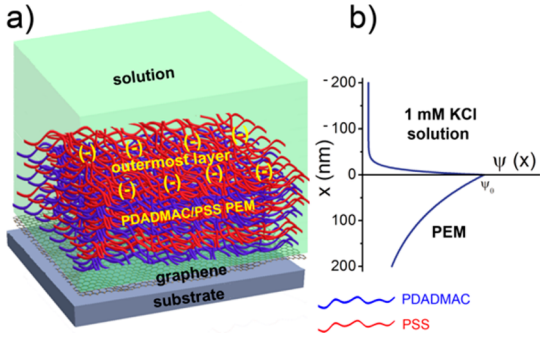

[a] x = 0 at the outermost polyelectrolyte layer.

Assuming that the overcompensated charges in the PEM film are located at the interface between the outermost layer and the solution (see Scheme 2a) and the charge magnitude of the outermost polyelectrolyte layer does not vary by increasing the number of layers, the linear Debye−Huckel (DH) theory can

DOI: 10.1021/acs.jpcc.7b11128
J. Phys. Chem. C 2018, 122, 10181−10188

be used to describe the potential, $\psi(x)$, inside the PEMs. The electrostatic screening of the outermost charged layer can be accounted as

$$\psi(x) = \psi_0 \exp(-\kappa_p x) \quad (1)$$

where x is the distance inside the PEM from the outermost layer ($x = 0$) to the graphene surface, ψ_0 the potential at the film/solution interface, and κ_p^{-1} the Debye screening length of the polyelectrolyte multilayer. For an aqueous solution at room temperature, κ^{-1} is given by[38]

$$k_p^{-1} = \left(4\pi\lambda_B \sum_i \rho_i z_i^2\right)^{-1/2} \quad (2)$$

where z_i and ρ_i are the valence and the density[39] of species i and $\lambda_B \approx 0.7$ nm is the Bjerrum length. It can be seen from eq 1 that if $x = \kappa_p^{-1}$ then $\psi = \psi_0 \exp(-1)$.

Figure 3 shows ΔV_i as a function of the number of layers for PEMs prepared at high ionic strength and measured at 1 mM

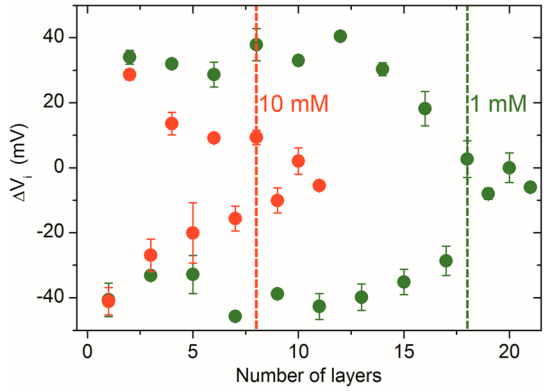

Figure 3. Change of the Dirac point, ΔV_i, as a function of the layers of PEMs prepared from polyelectrolyte solutions at high ionic strength (0.5 M KCl) and measured at 1 mM (green) and 10 mM KCl (red). The dashed lines indicate the number of layers where ΔV_i is equal to $\Delta V_{i0}/\exp(1)$. At this condition, the film thickness equals κ_p^{-1}.

(green) and 10 mM KCl (red). As the number of layers can be translated into film thickness, its correlation to ΔV_i allows a reliable estimation of the κ_p^{-1} value. Since ΔV_i is proportional to $\Delta\psi_s$, κ_p^{-1} can be estimated as the necessary film thickness where ΔV_i is equal to $\Delta V_{i0}/\exp(1)$. ΔV_{i0} is the Dirac point change after the adsorption of the first polyelectrolyte layer. The obtained κ_p^{-1} was 125 ± 10 and 36 ± 4 nm for 1 and 10 mM KCl, respectively. Notably, κ_p^{-1} is higher by 1 order of magnitude than κ_s^{-1} (which is 9.6 and 3.04 nm for 1 and 10 mM KCl). Subsequently, the concentration of mobile charges inside the PEM can be determined using eq 2. The concentration of mobile ions inside of the PEM was 0.0060 ± 0.0009 and 0.073 ± 0.015 mM for 1 and 10 mM KCl solutions, respectively.

3.3. Thermodynamic Model: Partition of Ions.

Although polymer interfaces such as PEG brushes were previously used to extend the sensing range of nanomaterial-based FETs,[8,20] little is known about the mechanism for increasing the Debye length. To shed light on this issue, a conceptually simple thermodynamic model to describe the partition of ions inside the PEM film was derived. In this model, we describe the interior of the film and neglect polymer–solution interface effects. Consider a solution containing water (w), water ions (H_3O^+ and OH^-), salt anions (−), and salt cations (+). These molecules can freely move in the solution. Inside the film their translational freedom is significantly reduced by the presence of the polymer in high density. Moreover, we assume the film is electroneutral due to polymer–polymer charge compensation.

The density of grand potential in either subsystem is

$$\beta\Omega^k = \sum_i \rho_i^k(\beta\mu_i^0 + \ln \rho_i^k v_w - 1) - \sum_i \rho_i^k \mu_i \quad (3)$$

with $\beta = 1/k_BT$, where T is the temperature. The superscript $k \in \{\text{sol, film}\}$ indicates whether we are looking at the solution or inside the film, and the index i runs over all mobile species. The first sum in eq 3 contains the self-energy and the translational entropy of these molecules. In these expressions, μ_i^0 is the standard chemical potential of the corresponding species, and ρ_i^k its density in either subsystem. The last term in eq 3 accounts for having the chemical potential of the molecules, μ_i, externally fixed and equal in both phases.

To the thermodynamic potential expressed in eq 3, we apply an incompressibility constraint in each fluid phase, which means that each element of volume is completely occupied by some molecular species. In the solution subsystem, this constraint can be expressed as

$$\rho_w^{sol} v_w + \rho_{H_3O^+}^{sol} v_{H_3O^+} + \rho_{OH^-}^{sol} v_{OH^-} + \rho_+^{sol} v_+ + \rho_-^{sol} v_- = 1 \quad (4)$$

while inside the film, the incompressibility implies

$$\rho_w^{film} v_w + \rho_{H_3O^+}^{film} v_{H_3O^+} + \rho_{OH^-}^{film} v_{OH^-} + \rho_+^{film} v_+ + \rho_-^{film} v_- = 1 - \phi_p \quad (5)$$

Optimizing the thermodynamic potential with respect to the densities of the free species leads to

$$\rho_i^k = a_i \exp(-\beta\pi^k v_i)$$

where $a_i = \exp(\beta\mu_i - \beta\mu_i^0)$ is the species activity and π^{sol} and π^{film} are the Lagrange multipliers introduced to ensure satisfaction of eq 4 and eq 5, respectively.

In the solution side, all the activities and π^{sol} can be calculated using the pH and the salt concentration of the solution, electroneutrality, and the incompressibility constraint, eq 4.

Inside the film, the only remaining unknown, π^{film}, can be determined by numerically solving eq 5. This equation is solved iteratively using a Jacobian-free Newton method. The volumes of the water molecule and its ions are $v_w = v_{H_3O^+} = v_{OH^-} = 0.03$ nm^3. Salt ions are considered spherical, and to calculate their volume we use their hydrated molecular radius, $r_h^+ = 0.316$ nm for K^+ and $r_h^- = 0.316$ nm for Cl^-.[40,41] Once the densities of all mobile species inside the LbL film are known, the Debye length can be calculated using eq 2. Notice that in our approach, the activities of the different free species are not parametrized, but they can be calculated though solving eq 4 and using the input concentrations.

In Figure 4a, κ_p^{-1} (solid lines) and κ_s^{-1} (dashed line) are plotted as a function of the KCl concentration in solution for different ϕ_p. The electrostatic screening inside the film strongly depends on the polymer volume fraction (ϕ_p) and the solution ionic strength. Polymer films with higher ϕ_p result in assemblies with lower (mobile) ion concentrations and larger κ_p^{-1}. Low

DOI: 10.1021/acs.jpcc.7b11128
J. Phys. Chem. C 2018, 122, 10181−10188

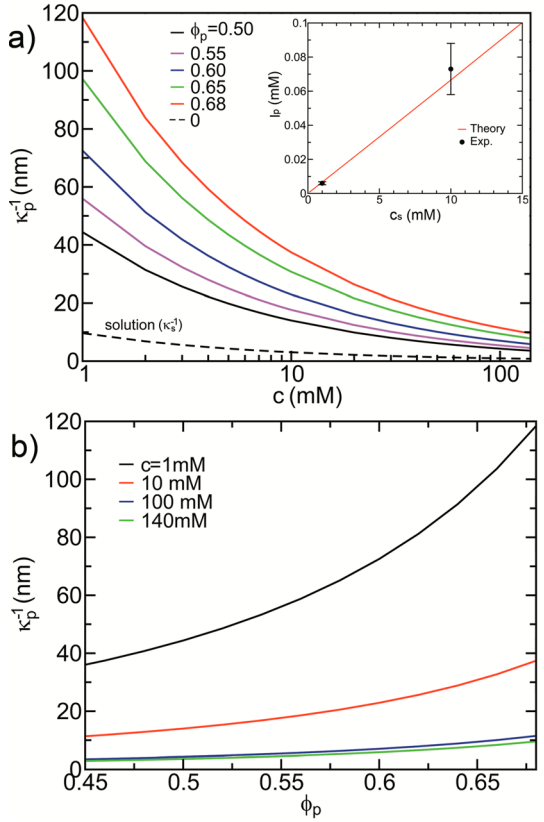

Figure 4. Theoretical predictions: (a) Debye length, κ_p^{-1}, as a function of the KCl concentration in the solution, c_s, for different polymer volume fractions, ϕ_p. Inset: Ionic strength of mobile ions inside the PDADMAC/PSS PEM, I_p, as a function of c_s. The red line and the black dots are the theoretical and experimental results, respectively. (b) κ_p^{-1} as a function of ϕ_p for different solution KCl concentrations.

hydrated films such as PDADMAC/PSS multilayer (with a ϕ_p of 0.68) present Debye lengths more than 1 order of magnitude higher than that of the solution in contact with the film: at 10 mM κ_p^{-1} is 37.4 nm while κ_s^{-1} is 3.07 nm. At 1 mM KCl, κ_p^{-1} is 118.4 nm while κ_s^{-1} is 9.6 nm. These theoretical results are in quantitative agreement with the experimental observations.

The ionic strength of mobile ions inside the PDADMAC/PSS PEM (I_p) as a function of the KCl concentration in the solution (c_s) is plotted in the inset of Figure 4a. The theoretical and experimental results are represented by a red line and black circles, respectively. A linear relation was observed between I_p and c_s. The slope of the linear regression is the square-root of the partition coefficient ($P_{p/s}$) between mobile ions inside the film and the solution (see the Supporting Information for details). The obtained value of $P_{p/s}$ was 4.9×10^{-5}. Furthermore, the theoretical results predict that $P_{p/s}$ significantly depends on the radius of the ions. This observation is consistent with the previously reported property of PDADMAC/PSS PEM when used as nanofiltration membranes for the separation of monovalent ions based on their size.[42]

As can be seen in Figure 4b, the phenomenon of extending κ_p^{-1} vanishes as the polymer density decreases. When ϕ_p decreases from 0.68 (PEM fillms) to 0.2 (like PEG brushes-modified surfaces) κ_p^{-1} decreases from 118 to 15.8 nm, for a 1 mM KCl solution. These results indicate that highly dense polymer interfaces have to be constructed if larger sensing ranges are needed.

The theoretical results explain that the increase of the electrostatic screening length is governed by the entropic cost of confining (mobile) ions inside the film. The nature of this phenomena is mainly based on three inherent features of these systems: (i) PDADMAC/PSS PEM polymer matrices are poorly hydrated (ϕ_p is higher than 0.6); (ii) the volume of hydrated salt ions is significantly larger than that of water molecules; (iii) there is no electrostatic driving force for the ions to absorb since the interdigitating oppositely charged polymers maintain electroneutrality inside the material. Because of these features, the entropic cost of ions partition from the solution to the film is high without any gain in electrostatic energy. As a consequence, the concentration of mobile ions in the PEM films can be markedly smaller than in solution. It is important to note that the basis of the Debye screening length increase by ions partition applies not only to PEM films but also to other polymer interfaces such as brushes and hydrogels.

The theoretical results predict that the construction of PDADMAC/PSS PEM on graphene could increase κ^{-1} from 0.82 to 9.6 nm in physiological environments. This sensing range may allow the determination of biomolecules of paramount importance in health care such as proteins and nucleic acids using clinic samples or implantable transistors. It should be noticed that one mandatory feature for the design of FET biosensor is the transport of the analyte through the film.[8] Although the permeation of biomacromolecules may be reduced by dense films, it was previously reported that some proteins (i.e., papain, lyzozyme, catalase, and other proteins) can be entrapped in PEM matrices.[43,44] On the other hand, these results also show that the integration of biorecognition motifs onto the graphene surface in a "multilayer format" can lead to an increased sensitivity of the gFET device.

All previous calculations were done at pH 7. To account for pH implication in Debye length increment, additional calculations were performed at pH values of 3, 5, and 9. The results are shown in Table 1. In our simple thermodynamic model, the only effect of pH is modifying the (bulk) solution composition. As PSS and PDADMAC are strong polyelectrolytes, slight changes in the pH should not significantly affect the LbL assembly, therefore supporting our assumption. Nevertheless, ionic strength changes and, with it, an increase in mobile ions inside the polyelectrolyte assembly should be considered. At 1 and 10 mM KCl, the concentration of H_3O^+ and OH^- should still be much lower than those of K^+ and Cl^-, even at pH 5 or 9, thus having little influence on the final results. However, H_3O^+ and OH^- have a smaller radius; consequently, the number of mobile ions inside the assembly could increase significantly at pH values below 4 or above 10 and consequently decrease the Debye length.

Table 1. Debye Length inside the Film for Different pH and Salt Concentrations

	Debye length, nm		
pH	[salt] = 1 mM	[salt] = 10 mM	[salt] = 140 mM
3	23.4	20.1	8.9
5	106.3	37.0	9.6
7	118.4	37.4	9.6
9	106.3	37.9	9.6

DOI: 10.1021/acs.jpcc.7b11128
J. Phys. Chem. C 2018, 122, 10181−10188

4. CONCLUSIONS

In conclusion, we demonstrated that polyelectrolyte multilayer films are capable to abruptly increase the sensing range of graphene-based FETs. The electrostatic screening length inside the film was obtained by correlating the film thickness and the potential drop during the construction of the assemblies. Interestingly, the Debye length inside the PEM film could be increased more than 1 order of magnitude. Our theoretical predictions using a thermodynamic model indicate that this behavior results mainly from the entropic cost of confining ions inside the polymer film. The electrostatic screening in the film strongly depends on the polymer density and the ionic strength of the solution. Of major importance for biosensing in clinical samples, PDADMAC/PSS multilayer films could increase the sensing range in physiological environments from 0.82 to 9.6 nm. In this way, by the use of this strategy the frontiers of FET sensing may be extended from small molecules to a broad variety of biomacromolecules such as proteins and nucleic acids. Lastly, the basis of the Debye screening length increase by ions partition can be also used to understand and extend the sensing range of nanomaterial-based FETs using other polymer interfaces such as brushes and hydrogels.

■ ASSOCIATED CONTENT

Supporting Information

The Supporting Information is available free of charge on the ACS Publications website at DOI: 10.1021/acs.jpcc.7b11128.

Scanning electron microscopy (SEM) images of graphene-based FETs and SPR/OWS substrates; further details on OWS and SPR measurements; water content calculation; partition-coefficient equitation (PDF)

■ AUTHOR INFORMATION

Corresponding Authors

*E-mail address: estebanpiccinini@inifta.unlp.edu.ar (E.P.); website: http://softmatter.quimica.unlp.edu.ar, https://www.facebook.com/SoftMatterLaboratory/.

*E-mail address: azzaroni@inifta.unlp.edu.ar (O.A.); website: http://softmatter.quimica.unlp.edu.ar, https://www.facebook.com/SoftMatterLaboratory/.

ORCID

Josef Breu: 0000-0002-2547-3950

Jakub Dostalek: 0000-0002-0431-2170

Omar Azzaroni: 0000-0002-5098-0612

Author Contributions

⊥These authors contributed equally to this work and should be considered as cofirst authors.

Notes

The authors declare no competing financial interest.

■ ACKNOWLEDGMENTS

This work was supported by CONICET, ANPCyT (PICT-2010-2554, PICT-2013-0905, PICT-2014-3377), the Austrian Institute of Technology GmbH (AIT-CONICET Partner Group, Exp. 4947/11, Res. No. 3911, 28-12-2011), Universidad Nacional de La Plata (UNLP), and the Austrian Federal Ministry for Transportation, Innovation and Technology (GZ BMVIT-612.166/0001-III/I1/2010), by the FFG within the comet program, and from the governments of Lower and Upper Austria. E.P. and S.A. acknowledge CONICET for a scholarship. G.S.L. and O.A. are staff researchers of CONICET. We thank Dr. Waldemar Marmisollé for helpful discussions.

■ REFERENCES

(1) Cui, Y.; Wei, Q.; Park, H.; Lieber, C. M. Nanowire Nanosensors for Highly Sensitive and Selective Detection of Biological and Chemical Species. *Science* **2001**, *293*, 1289−1292.

(2) Fu, W.; Jiang, L.; van Geest, E. P.; Lima, L. M. C.; Schneider, G. F. Sensing at the Surface of Graphene Field-Effect Transistors. *Adv. Mater.* **2017**, *29*, 1603610.

(3) Zhang, A.; Lieber, C. M. Nano-Bioelectronics. *Chem. Rev.* **2016**, *116*, 215−257.

(4) Yan, F.; Zhang, M.; Li, J. Solution-Gated Graphene Transistors for Chemical and Biological Sensors. *Adv. Healthcare Mater.* **2014**, *3*, 313−331.

(5) Zhang, M.; Liao, C.; Mak, C. H.; You, P.; Mak, C. L.; Yan, F. Highly Sensitive Glucose Sensors Based on Enzyme-Modified Whole-Graphene Solution-gated Transistors. *Sci. Rep.* **2015**, *5*, 8311.

(6) Piccinini, E.; Bliem, C.; Reiner-Rozman, C.; Battaglini, F.; Azzaroni, O.; Knoll, W. Enzyme-Polyelectrolyte Multilayer Assemblies on Reduced Graphene Oxide Field-Effect Transistors for Biosensing Applications. *Biosens. Bioelectron.* **2017**, *92*, 661−667.

(7) Larisika, M.; Kotlowski, C.; Steininger, C.; Mastrogiacomo, R.; Pelosi, P.; Schütz, S.; Peteu, S. F.; Kleber, C.; Reiner-Rozman, C.; Nowak, C.; Knoll, W. Electronic Olfactory Sensor Based on *A. mellifera* Odorant-Binding Protein 14 on a Reduced Graphene Oxide Field-Effect Transistor. *Angew. Chem., Int. Ed.* **2015**, *54*, 13245−13248.

(8) Gao, N.; Gao, T.; Yang, X.; Dai, X.; Zhou, W.; Zhang, A.; Lieber, C. M. Specific Detection of Biomolecules in Physiological Solutions Using Graphene Transistor Biosensors. *Proc. Natl. Acad. Sci. U. S. A.* **2016**, *113*, 14633−14638.

(9) Stern, E.; Vacic, A.; Rajan, N. K.; Criscione, J. M.; Park, J.; Ilic, B. R.; Mooney, D. J.; Reed, M. a.; Fahmy, T. M. Label-Free Biomarker Detection from Whole Blood. *Nat. Nanotechnol.* **2010**, *5*, 138−142.

(10) Xu, S.; Zhan, J.; Man, B.; Jiang, S.; Yue, W.; Gao, S.; Guo, C.; Liu, H.; Li, Z.; Wang, J.; et al. Real-Time Reliable Determination of Binding Kinetics of DNA Hybridization Using a Multi-Channel Graphene Biosensor. *Nat. Commun.* **2017**, *8*, 14902.

(11) Cai, B.; Wang, S.; Huang, L.; Ning, Y.; Zhang, Z.; Zhang, G. Ultrasensitive Label-Free Detection of PNA-DNA Hybridization by Reduced Graphene Oxide Field-Effect Transistor Biosensor. *ACS Nano* **2014**, *8*, 2632−2638.

(12) Patolsky, F.; Zheng, G.; Hayden, O.; Lakadamyali, M.; Zhuang, X.; Lieber, C. M. Electrical Detection of Single Viruses. *Proc. Natl. Acad. Sci. U. S. A.* **2004**, *101*, 14017−14022.

(13) Balasubramanian, K.; Kern, K. 25th Anniversary Article: Label-Free Electrical Biodetection Using Carbon Nanostructures. *Adv. Mater.* **2014**, *26*, 1154−1175.

(14) Stern, E.; Wagner, R.; Sigworth, F. J.; Breaker, R.; Fahmy, T. M.; Reed, M. A. Importance of the Debye Screening Length on Nanowire Field Effect Transistor Sensors. *Nano Lett.* **2007**, *7*, 3405−3409.

(15) Soikkeli, M.; Kurppa, K.; Kainlauri, M.; Arpiainen, S.; Paananen, A.; Gunnarsson, D.; Joensuu, J. J.; Laaksonen, P.; Prunnila, M.; Linder, M. B.; et al. Graphene Biosensor Programming with Genetically Engineered Fusion Protein Monolayers. *ACS Appl. Mater. Interfaces* **2016**, *8*, 8257−8264.

(16) Elnathan, R.; Kwiat, M.; Pevzner, A.; Engel, Y.; Burstein, L.; Khatchtourints, A.; Lichtenstein, A.; Kantaev, R.; Patolsky, F. Biorecognition Layer Engineering: Overcoming Screening Limitations of Nanowire-Based FET Devices. *Nano Lett.* **2012**, *12*, 5245−5254.

(17) Maehashi, K.; Katsura, T.; Kerman, K.; Takamura, Y.; Matsumoto, K.; Tamiya, E. Label-Free Protein Biosensor Based on Aptamer-Modified Carbon Nanotube Field-Effect Transistors. *Anal. Chem.* **2007**, *79*, 782−787.

(18) Kulkarni, G. S.; Zhong, Z. Detection beyond the Debye Screening Length in a High-Frequency Nanoelectronic Biosensor. *Nano Lett.* **2012**, *12*, 719−723.

(19) Kulkarni, G. S.; Zang, W.; Zhong, Z. Nanoelectronic Heterodyne Sensor: A New Electronic Sensing Paradigm. *Acc. Chem. Res.* **2016**, *49*, 2578−2586.
(20) Gao, N.; Zhou, W.; Jiang, X.; Hong, G.; Fu, T.-M.; Lieber, C. M. General Strategy for Biodetection in High Ionic Strength Solutions Using Transistor-Based Nanoelectronic Sensors. *Nano Lett.* **2015**, *15*, 2143−2148.
(21) Decher, G.; Hong, J. D. Buildup of Ultrathin Multilayer Films by a Self-Assembly Process: II. Consecutive Adsorption of Anionic and Cationic Bipolar Amphiphiles and Polyelectrolytes on Charged Surfaces. *Ber. Bunsenges. Phys. Chem.* **1991**, *95*, 1430−1434.
(22) Decher, G. Fuzzy Nanoassemblies: Toward Layered Polymeric Multicomposites. *Science* **1997**, *277*, 1232−1237.
(23) Ariga, K.; Hill, J. P.; Ji, Q. Layer-by-Layer Assembly as a Versatile Bottom-up Nanofabrication Technique for Exploratory Research and Realistic Application. *Phys. Chem. Chem. Phys.* **2007**, *9*, 2319−2340.
(24) Piccinini, E.; Pallarola, D.; Battaglini, F.; Azzaroni, O. Recognition-Driven Assembly of Self-Limiting Supramolecular Protein Nanoparticles Displaying Enzymatic Activity. *Chem. Commun.* **2015**, *51*, 14754−14757.
(25) Decher, G.; Schlenoff, J. B. *Multilayer Thin Films: Sequential Assembly of Nanocomposite Materials*, second ed.; Decher, G., Schlenoff, J. B., Eds.; WILEY-VCH Verlag GmbH & Co: Weinheim, Germany, 2012.
(26) Maza, E.; Tuninetti, J. S.; Politakos, N.; Knoll, W.; Moya, S.; Azzaroni, O. pH-Responsive Ion Transport in Polyelectrolyte Multilayers of Poly (diallyldimethylammonium chloride)-(PDADMAC) and Poly (4-styrenesulfonic acid-*co*-maleic acid)(PSS-MA) Bearing Strong-and Weak Anionic Groups. *Phys. Chem. Chem. Phys.* **2015**, *17*, 29935−29948.
(27) Tang, K.; Besseling, N. A. M. Formation of Polyelectrolyte Multilayers: Ionic Strengths and Growth Regimes. *Soft Matter* **2016**, *12*, 1032−1040.
(28) Iturri Ramos, J. J.; Stahl, S.; Richter, R. P.; Moya, S. E. Water Content and Build-up of Poly(diallyldimethylammonium chloride)/Poly(sodium 4-styrenesulfonate) and Poly(allylamine hydrochloride)/Poly(sodium 4-styrenesulfonate) Polyelectrolyte Multilayers Studied by an In Situ Combination of a Quartz Crystal Microbalance with Dissipation Monitoring and Spectroscopic Ellipsometry. *Macromolecules* **2010**, *43*, 9063−9070.
(29) Wang, Y. Y.; Burke, P. J. Polyelectrolyte Multilayer Electrostatic Gating of Graphene Field-Effect Transistors. *Nano Res.* **2014**, *7*, 1650−1658.
(30) Smith, R. N.; Reven, L.; Barrett, C. J. ^{13}C Solid-State NMR Study of Polyelectrolyte Multilayers. *Macromolecules* **2003**, *36*, 1876−1881.
(31) Artyukhin, A. B.; Stadermann, M.; Friddle, R. W.; Stroeve, P.; Bakajin, O.; Noy, A. Controlled Electrostatic Gating of Carbon Nanotube FET Devices. *Nano Lett.* **2006**, *6*, 2080−2085.
(32) Lösche, M.; Schmitt, J.; Decher, G.; Bouwman, W. G.; Kjaer, K. Detailed Structure of Molecularly Thin Polyelectrolyte Multilayer Films on Solid Substrates as Revealed by Neutron Reflectrometry. *Macromolecules* **1998**, *31*, 8893−8906.
(33) Schlenoff, J. B.; Ly, H.; Li, M. Charge and Mass Balance in Polyelectrolyte Multilayers. *J. Am. Chem. Soc.* **1998**, *120*, 7626−7634.
(34) Xie, A. F.; Granick, S. Local Electrostatics with a Polyelectrolyte Multilayer with Embedded Weak Polyelectrolyte. *Macromolecules* **2002**, *35*, 1805−1813.
(35) Schönhoff, M.; Ball, V.; Bausch, A. R.; Dejugnat, C.; Delorme, N.; Glinel, K.; Klitzing, R. v.; Steitz, R. Hydration and Internal Properties of Polyelectrolyte Multilayers. *Colloids Surf., A* **2007**, *303*, 14−29.
(36) Neff, P. A.; Naji, A.; Ecker, C.; Nickel, B.; Klitzing, R. v.; Bausch, A. R. Electrical Detection of Self-Assembled Polyelectrolyte Multilayers by a Thin Film Resistor. *Macromolecules* **2006**, *39*, 463−466.
(37) Neff, P. A.; Wunderlich, B. K.; Klitzing, R. v.; Bausch, A. R. Formation and Dielectric Properties of Polyelectrolyte Multilayers Studied by a Silicon-on-Insulator Based Thin Film Resistor. *Langmuir* **2007**, *23*, 4048−4052.
(38) Israelachvili, J. *Intermolecular and Surface Forces*, 3rd edition; Israelachvili, J., Ed.; Academic Press: New York, 2011.
(39) ρ is the number of molecules per nm^3. The relation of ρ and the molar concentration, M, is $\rho = \frac{MN_A}{10^{24}}$. N_A is Avogadró's constant.
(40) Brady, G. W.; Krause, J. T. Structure in Ionic Solutions. I. *J. Chem. Phys.* **1957**, *27*, 304−308.
(41) Marcus, Y. Ionic Radii in Aqueous Solutions. *Chem. Rev.* **1988**, *88*, 1475−1498.
(42) Hong, S. U.; Malaisamy, R.; Bruening, M. L. Separation of Fluoride from Other Monovalent Anions Using Multilayer Polyelectrolyte Nanofiltration Membranes. *Langmuir* **2007**, *23*, 1716−1722.
(43) Uhlig, K.; Madaboosi, N.; Schmidt, S.; Jäger, M. S.; Rose, J.; Duschl, C.; Volodkin, D. V. 3d Localization and Diffusion of Proteins in Polyelectrolyte Multilayers. *Soft Matter* **2012**, *8*, 11786−11789.
(44) Sustr, D.; Duschl, C.; Volodkin, D. A FRAP-Based Evaluation of Protein Diffusion in Polyelectrolyte Multilayers. *Eur. Polym. J.* **2015**, *68*, 665−670.

DOI: 10.1021/acs.jpcc.7b11128
J. Phys. Chem. C 2018, 122, 10181−10188